Macromolecules

Article

pubs.acs.org/Macromolecules

One-Step Electrospinning To Produce Nonsolvent-Induced Macroporous Fibers with Ultrahigh Oil Adsorption Capability

Po-Yu Chen and Shih-Huang Tung*

Institute of Polymer Science and Engineering, National Taiwan University, Taipei 10617, Taiwan

ABSTRACT: The demand for an efficient method to clean spreading oil on water is increasingly urgent due to the frequent occurrence of oil spill accidents around the world. In this work, we used a simple one-step electrospinning technique without the requirement of post-treatments to fabricate polystyrene (PS) fibrous sorbents that show exceptional oil adsorption capability. This method involves the dissolution of PS in cosolvents composed of a good solvent, chlorobenzene, and a nonsolvent, DMSO, for electrospinning. The size of the PS fibers electrospun from the cosolvents is rather uniform, and more importantly, the nonsolvent induces a highly porous structure throughout the fibers during the drying process. The porous structure imparts superhydrophobic surface to the fibrous mats, and thus the fibers can selectively adsorb oils while repel water. Furthermore, both the capacity and the rate of oil adsorption are greatly enhanced for the sorbents made of the porous fibers, in contrast to pore-free ones. The oil adsorption capability is closely dependent on the fiber size and the porous morphology, which can be simply controlled by adjusting the compositions of polymer solutions.

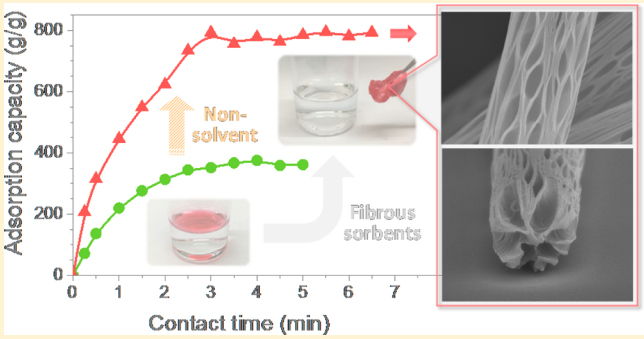

1. INTRODUCTION

Large-scale oil spill accidents have caused huge economic losses and severe environmental damages. The cleanup of the spilled oils is an urgent and strenuous task. One of the efficient methods for oil cleanup is the solidification of the oils, i.e., the use of hydrophobic sorbents to transfer the spilled oils from liquid to a semisolid phase that can be much easily retrieved. The required properties of ideal sorbent materials for oil spill cleanup include an appropriate hydrophobicity and a high specific surface area for increasing the performance in oil selectivity, sorption capacity, sorption rate, and retention time. Moreover, the buoyancy and durability of sorbents in aqueous media, the reusability or biodegradability of materials, and the recoverability of oil from sorbents should also be taken into account.[1]

The sorbents used for oil spill cleanup include inorganic mineral materials and natural/synthetic organic materials,[2] among which synthetic polymer fibers are particularly suitable because of the controllable hydrophobicity, high specific surface area, lightweight, simple manufacturing, and low cost,[3] especially the porous fibers with large overall specific surface area that can increase the efficiency and capacity of oil adsorption.[4,5] The electrospinning technique is a straightforward method to produce micro/nanoscale fibers. Various methods have been developed to increase the porosity of electrospun fibers, such as electrospinning of polymer blends and subsequent selective removal one of the polymer phases,[6] the use of bath collector,[7,8] and the use of additives.[9] However, those methods generally require post-electrospinning treatment, therefore lacking a simplicity for mass production.

In the field of polymer membranes, phase separation is a common strategy adopted to produce porous structures. Based on the phase separation mechanisms, the strategy can be divided into three major categories: vapor-induced phase separation (VIPS), thermally induced phase separation (TIPS), and nonsolvent-induced phase separation (NIPS). In the VIPS method, vapors (usually water) are condensed as nonsolvents that cause originally homogeneous solutions to phase separate and porous structures can be obtained after the removal of solvents.[10,11] VIPS also occurs in the electrospinning process. Solvent evaporation cools down the jet surface and the moisture condenses from the atmosphere, thus initiating the nucleation and growth of the water-rich phase floating on the solution, which subsequently leaves pores on the fiber surface.[5,12−16] In the TIPS method, a homogeneous polymer solution is first prepared at an elevated temperature and then rapidly cooled to a temperature where the solvent quality turn to be poor to polymer and phase separation occurs.[17] This method can be applied to produce electrospinning porous polymer fibers by controlling the collector at relatively low temperature to induce phase separation.[18] NIPS is also called immersion precipitation method by which a cast polymer solution is immersed in a nonsolvent bath to initiate phase separation.[19] For the electrospinning technique, it has been reported that nonsolvents can be premixed in polymer solutions with an appropriate amount that does not cause

Received: December 14, 2016
Revised: February 23, 2017
Published: March 6, 2017

DOI: 10.1021/acs.macromol.6b02696
Macromolecules 2017, 50, 2528−2534

phase separation before electrospinning. During the subsequent solidification process, the composition changes and falls into the phase separation region because of the different volatility between solvent and nonsolvent, and porous structures can be created.[20−22] However, the fibers produced by this method in previous studies were generally not uniform.

The common method for manufacturing porous electrospun fibers is VIPS. However, because the moisture condenses into water drops mainly on the surface of solutions, the remaining pores are generally isolated and only formed on fiber surface. Therefore, the increase in the pore volume and specific surface area is limited, and it has been shown that the oil adsorption capacity of fibers produced by the VIPS method does not significantly increase from that of smooth fibers.[5] Although the TIPS method can be used to produce pores throughout fibers, this method needs post-treatments to remove residual solvents because the fibers are not completely dried in the electrospinning process. In this study, we combined NIPS concept and electrospinning technique to produce uniform porous polystyrene (PS) fibrous sorbents. The fibers with macroporous structure throughout can be fabricated by a simple one-step electrospinning process from solutions in which a good solvent, chlorobenzene (CB), and a nonsolvent, DMSO, are premixed. Silicone oil, pump oil, sunflower oil, and diesel with different viscosities are used as model oils to investigate the adsorption characteristics of as-spun fibrous sorbents. By tuning the compositions of polymer solutions, fibrous sorbents with different porous morphology and different adsorption ability can be obtained. The adsorption capacity of the highly porous PS fibrous sorbents can reach up to 900 g/g, showing a great potential for the use in the application of oil spill cleanup.

2. EXPERIMENTAL SECTION

2.1. Materials. Polystyrene (PS, $M_w \sim 350\,000$ g/mol, PDI = 2.06) was purchased from Sigma-Aldrich. Chlorobenzene (CB, ACS Reagent grade) and dimethyl sulfoxide (DMSO, ACS Reagent grade) were purchased from J.T. Baker. Tetrabutylammonium perchlorate (TBAP, >98%) was purchased from Tokyo Chemical Industry Co., Ltd. All chemicals were used as received.

2.2. Electrospinning Process. To prepare the solutions for electrospinning, PS was mixed in cosolvents of CB and DMSO at different ratios, followed by magnetic stirring at 50 °C for 12 h to obtain homogeneous solutions. The electrospinning fibers were prepared using a single-capillary spinneret. The polymer solutions were fed into a syringe pump (YSP-101, YMC) connected to a metallic needle (22 gauge, Hamilton), with a feed rate of 0.5 mL/h. The metallic needle was connected to a high-voltage power supply (chargemaster VCM30-P, Simco-Ion), and a piece of aluminum foil was placed 15 cm below the tip of the needle to collect the fibers. The applied voltage was 4−10 kV. All the experiments were carried out at room temperature (20−30 °C) and a relative humidity of 50−70%. The sample codes of the electrospun fibers named from the compositions of the corresponding solutions are listed in Table 1.

2.3. SEM. The morphologies of the as-spun fibers were characterized by a field-emission scanning electron microscopy (JSM-6330F, JEOL). SEM images were captured at an accelerating voltage of 10 kV. For cross-sectional imaging, the fibers were transferred onto silicon wafer, and then the fiber-covered wafer was cut into two pieces to break the fibers and reveal the cross sections. Before imaging, the samples were sputtered with platinum.

2.4. Phase Behaviors of the Solutions. A series of solutions with varying compositions of PS, CB, and DMSO were prepared and sealed in glass bottles. The solutions were first mixed at 50 °C and stirred until clear homogeneous solutions were obtained. The solutions were then cooled down and kept at room temperature. The solutions with the compositions that were in the stable regime at room temperature remained transparent, while those in the unstable regime turned to be cloudy, indicating the occurrence of phase separation. The liquid−liquid demixing boundary at room temperature was determined by the cloud point method.

Table 1. Solution Compositions and the Characteristics of As-Spun Fibers

	DMSO/CB (v/v)	PS conc (mg/mL)	TBAP (w/v)	fiber diameter (μm)	contact angle (°)
D0T	0/100	300	1%	0.62 ± 0.04	136.4 ± 3.2
D20	20/80	300	0	1.63 ± 00.06	148.9 ± 2.1
D30	30/70	300	0	2.85 ± 0.14	155.1 ± 4.8
D40	40/60	250	0	2.35 ± 0.22	152.3 ± 5.1
D15T	15/85	300	1%	0.89 ± 0.02	145.6 ± 0.9
D30T	30/70	300	1%	1.95 ± 0.14	153.8 ± 2.8

2.5. Mercury Intrusion Porosimetry. The pore size distributions of fibrous sorbents were measured using the mercury porosimeter AutoPore IV 9520, Micromeritics. The pressure (P) was applied ranging from 0.1 to 60 000 psia, and samples were equilibrated for 15 s at each pressure. The pressure was converted to pore diameter (D) by the Washburn equation assuming cylindrical pore geometry[23]

$$D = \frac{-4\gamma \cos\theta}{P} \tag{1}$$

where the surface tension (γ) of mercury is 485.000 dyn/cm and the contact angle (θ) was set to be 130°. The dependence of the cumulative specific intrusion volume (V) of mercury on the pore diameter was first determined. The distribution function of pore size was then calculated by differentiating the cumulative specific intrusion volume with respect to the pore diameter (dV/dD). The distribution curve of pore size is displayed as dV/dD against D.[24,25]

2.6. Water Contact Angle Tests. The static water contact angle was investigated by the Model 100SB contact angle goniometer from Sindatek Instruments Co., Ltd. The contact angle was determined by the Young−Laplace model and averaged from the measurements at least five times on different locations of sample surface at room temperature.

2.7. Oil Adsorption Tests. The maximum oil adsorption capacity of PS fiber sorbents was carried out using the following method. The electrospun fibrous sorbents were carefully removed from the aluminum foils by a gentle blow of compressed air to avoid the damage of the as-spun format of fibers. Approximate 10 mg of fibrous sorbents was placed in a glass beaker filled with 30 mL of oil. After adsorption for 1 h, the wet sorbent was removed from the oil bath and drained for 1 min. The oil adsorption capacity of the sorbent, Q (g/g), was determined by the equation

$$Q = \frac{m - m_0}{m_0} \tag{2}$$

where m is the total mass of the wet sorbent after 1 min draining and m_0 is the mass of the sorbent before adsorption. Each sample was independently measured for at least three times. The dependence of the adsorption capacity on time was determined by a similar process, except that the mass of the wet sorbent was weighed at a regular interval without the draining process.

3. RESULTS AND DISCUSSION

3.1. Electrospinnability of Polystyrene Solutions. Because of the low dielectric constant, chlorobenzene (CB) alone is not an appropriate solvent for electrospinning and the organic salts, such as tetrabutylammonium perchlorate (TBAP), are commonly added to enhance the conductivity of the solutions.[26−28] The addition of high dielectric constant solvents as cosolvents, such as DMSO, is another efficient way to increase the overall conductivity.[29] These additives, on one hand, enhance the electrospinnability of the solution and

DOI: 10.1021/acs.macromol.6b02696
Macromolecules 2017, 50, 2528−2534

produce bead-free fibers, but on the other hand, they may change the solvent quality to polymers as well as the viscosity and the surface tension of solutions, which are all critical parameters for electrospinning.

In this work, we used the cosolvents with varying ratios of CB and DMSO to electrospin PS fibers. The dependence of the fiber structure on PS concentration and DMSO volume fraction in cosolvents is shown in Figure 1. Since the conductivities of

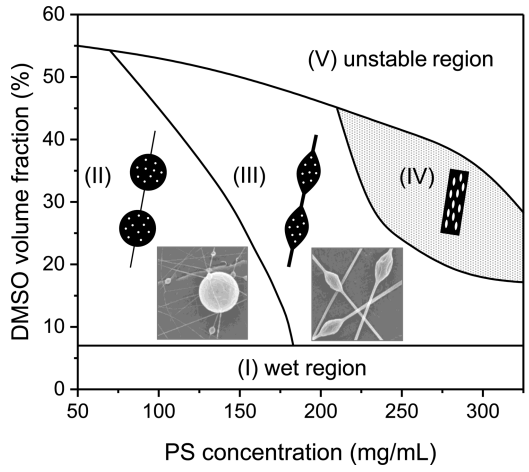

Figure 1. Dependence of fiber structures on DMSO volume fraction in cosolvents and PS concentration: (I) wet region where solvents are not completely dried after electrospinning, (II) beads or spherical bead fibers, (III) spindle-like bead fibers, (IV) uniform porous fibers, and (V) unstable region where the solutions are not electrospinnable.

the cosolvents with small amounts of DMSO are low and unable to carry sufficient charges to expedite evaporation of solvent by repulsive forces,[30,31] the electrospun samples in the region below ~7% DMSO (region I) cannot be dried completely after electrospinning. Note that the addition of TBAP in this region can improve the conductivity and make the electrospinning possible, which will be discussed later. In the range of DMSO fraction between 7% and 55%, the conductivity is increased and becomes feasible for electrospinning. The electrospun structure in this range depends on the PS concentration. At low PS concentration (region II), the entanglement of polymer chains is insufficient to hold a continuous, uniform liquid jet and only discontinuous beads or strings of spherical beads are produced. At intermediate PS concentration (region III), the stretching force can partially transfer to polymer chains through the entanglements and fibers with spindle-like beads are obtained. Only in the region of high PS concentration (region IV) can bead-free porous fibers be successfully produced. Since DMSO is a nonsolvent to PS, at DMSO fraction above 55% (region V), the solutions become unstable and tend to phase separate before electrospinning and therefore unable to be spun into fibers.

3.2. Morphologies and Pore Sizes of As-Spun Fibers.

The SEM images of as-spun PS fibers and their cross sections electrospun from 250−300 mg/mL solutions are shown in Figure 2. D0T fibers were electrospun from CB solution without DMSO but with 1% TBAP. As mentioned in section 3.1, CB solvent alone cannot be used to produce dry PS fibers, and the addition of TBAP is required to increase conductivity and electrospinnability. The surface of D0T fibers is smooth and featureless, with a diameter ~600 nm (Figure 2a). D20, D30, and D40 were produced from the cosolvents with 20%, 30%, and 40% of DMSO, respectively. D20 fibers show small and uniform ellipse-shaped pores randomly distributed on the surface (Figure 2b). The diameter of the fibers is ~1.5 μm, and the pore size on the surface is 100−300 nm. As the DMSO fraction increases to 30%, the fiber diameter increases to ~2.5 μm, and it is interesting that pores with various sizes and shapes appear on the surface (Figure 2c). The large lenticular or ellipse pores are aligned along the fiber axis, with a length 2−3 μm, and the size of smaller pores is 100−800 nm. In the case of D40 fibers, the pores further grow along the fiber axis and coalesce into continuous channels, resulting in a churro-like structure (Figure 2d). It is apparent that the pore size increases with increasing DMSO fraction, indicating that the nonsolvent must play an important role in the formation of the pores. Moreover, the shape and orientation of the pores are affected by the stretching forces.

The cross sections of the fibers are revealed in the bottom SEM images of Figure 2. D0T fibers show a loose structure in the core surrounded by a dense skin layer ~100 nm in thickness (Figure 2e). For D20 fibers whose porous surface looks similar to that produced by the VIPS method, beneath the relatively dense porous surface, large holes with ellipse cross sections grow from the small pores on surface to the center of

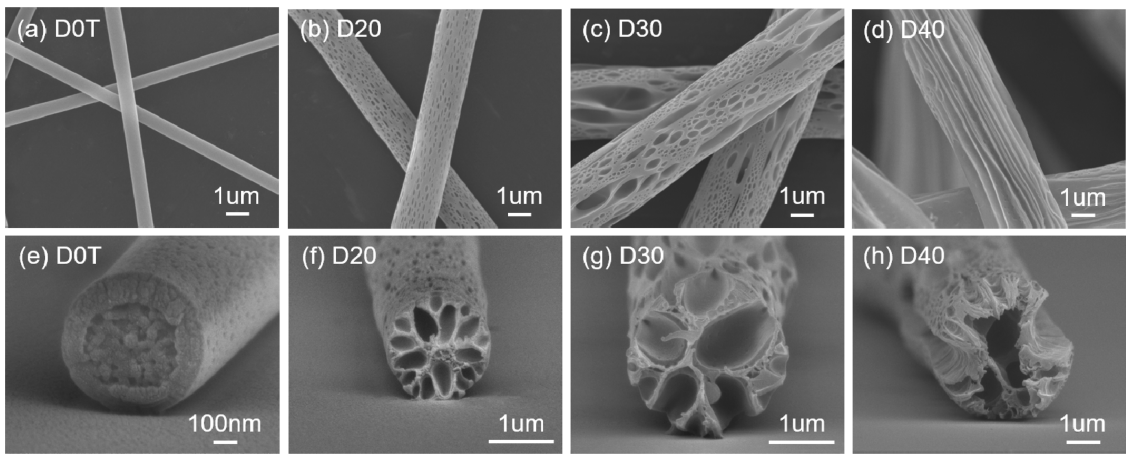

Figure 2. SEM micrographs of the surfaces (a−d) and the cross sections (e−h) of the as-spun PS fibers fabricated from solutions with varying compositions.

DOI: 10.1021/acs.macromol.6b02696
Macromolecules 2017, 50, 2528−2534

the fibers (Figure 2f), unlike the effect of the moisture condensation in the VIPS method that only causes pores on the surface.[5,12−16] With more nonsolvent DMSO in the cosolvent, D30 fibers show larger holes inside the fibers, and the hole entrance on the surface greatly expands, too (Figure 2g). This suggests that the holes formed inside the fibers are closely related the amount of the nonsolvent. Different from D20 and D30 fibers, although the holes inside D40 fibers join to form even larger ones, they are mostly isolated and less open to the air (Figure 2h). The continuous channels only appear on the surface, not deep into the fibers.

We had also incorporated TBAP into the cosolvents to further enhance the solvent conductivity. The SEM images of D15T fiber electrospun from the cosolvent of 15% DMSO and 1% TBAP are shown in Figures 3a and 3c. The morphology of

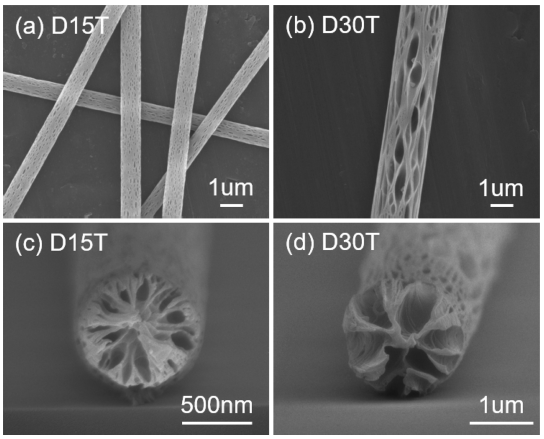

Figure 3. SEM micrographs of the surfaces (a, b) and cross sections (c, d) of the as-spun D15T and D30T fibers.

the fibers, i.e., the porous surface and the holes inside the fibers, is similar to that of D20, except that the fiber diameter is smaller, ∼1 μm. As shown in Figures 3b and 3d, the morphology of D30T fibers is analogous to that of D30, but the pore size on the surface is more uniform and the diameter is smaller, ∼2 μm. The thinner size of the fibers is due to the enhancement of solvent conductivity.[26] By combing the polar nonsolvent and the organic salt, we can produce electrospun fibers with small diameters and highly porous structures which, as will be discussed later, provides the fibers an exceptional ability to adsorb oils. Note that for the cosolvents with DMSO fraction >35%, addition of 1% TBAP turns the concentrated PS solutions to be cloudy and the solutions become infeasible for electrospinning, indicating that the solutions with TBAP phase separate at a lower fraction of DMSO in cosolvents than those without TBAP.

The mercury porosimeter was used to quantify the pore size distributions of the fibrous mats, as shown in Figure 4. The peaks between 10^4 and 10^3 nm represent the larger void space between the fibers. The thicker fibers, including D20 and D30, result in larger interfibrous void sizes around 10^4 nm while the thinner fibers, D0T, D15T, and D30T, exhibit a smaller void space around 10^3 nm. Note that the voids between fibers should have been compressed by the applied pressure upon measurements, and thus the void sizes obtained in this range may not reflect the real sizes of the undisturbed mats. The broad humps between 10^3 and 10^1 nm for D30 and D30T are supposed to be given by the microscale pores on the fibers,

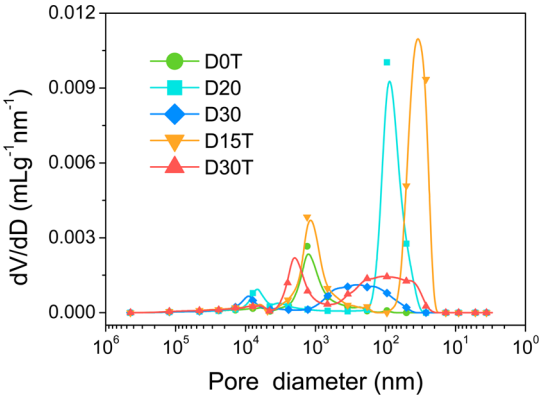

Figure 4. Pore size distributions of the fibrous mats.

consistent with the varying sizes and shapes of pores throughout the fibers observed by SEM in Figures 2 and 3. D20 and D15T show sharp peaks between 10^2 and 10^1 nm, indicating rather uniform nanoscale pores on the fibers, which also well agrees with the SEM images. As expected, the porous fibers like D20, D30, D15T, and D30T give rise to two main size distributions: one from the voids between fibers and the other from the pores on the fibers. In contrast, the pore-free D0T fibers only show one peak that comes from the voids between fibers.

3.3. Mechanism. During the electrospinning process, the solvent evaporates from the liquid jet and the polymer quickly solidifies from the solution. In addition to the simple drying process, since the present systems contain nonsolvent, the effect of phase separation during solvent evaporation has to be taken into account. To clarify the mechanism for the formation of macroporous fibers, we examined the phase behaviors of PS/CB/DMSO ternary system based on weight fraction at room temperature as shown in Figure 5. The phase diagram is divided

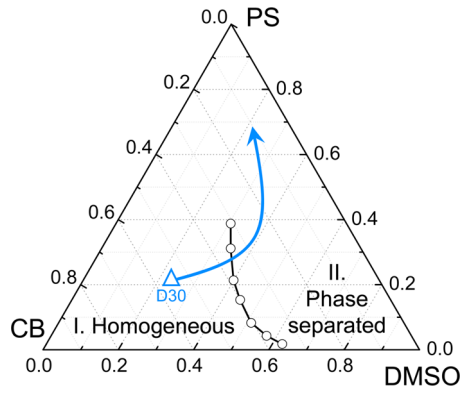

Figure 5. Phase diagram of the PS/CB/DMSO ternary system based on weight fraction at room temperature. The D30 solution is used as an example to illustrate the compositional change during solidification process.

into two regions by liquid−liquid demixing line determined by the compositions at which the solutions turn to be cloudy. The solutions in region I are homogeneous and transparent while those in region II phase separate into two liquid phases. Taking D30 sample as an example, the composition of the original solution is labeled in Figure 5. As solvent evaporates, two effects may involve to change the solvent quality. First, because of the higher evaporation rate of CB, the fraction of DMSO in

DOI: 10.1021/acs.macromol.6b02696
Macromolecules 2017, 50, 2528−2534

solutions increases with time. The solution thus follows the path to cross the liquid−liquid demixing line and phase separate into polymer-rich and solvent-rich phases. Second, the evaporation of solvent causes the condensation of moisture into liquid water, a nonsolvent that dissolves in DMSO to further lower the solvent quality to PS, which in turn accelerates the phase separation process.

For the D0T sample without DMSO, the effect of phase separation is not significant during drying process. The surface of the liquid jet dries first to form a dense skin, and the evaporation of the remaining CB leads to the loose structure in the core. In the presence of DMSO, the final morphology of the electrospun fibers is determined by the competition between the drying rate and the phase separation rate. In the case of D20 with a low fraction of DMSO, the outer solution slightly crosses the demixing line upon initial drying, which causes the formation of the nanoscale pores on the surface. The phase separation aggravates with time and the solvent-rich phases eventually turn into large holes inside the fibers as solvent dries out. As the DMSO fraction increases, the phase separation occurs earlier. Larger pores thus appear on the surface and propagate into the interior of the fibers, as seen for D30 fibers. The phase separation domains tend to be spheroidal in nature to reduce interfacial free energy. However, because of the elongation in the axial direction under stretching and the shrinkage in radial direction upon drying, the domains are oriented along the fiber axis and deformed into ellipsoid both on the surface and in the interior of the fibers. For D40 sample, the DMSO fraction is so high that the composition of the solution is close to the demixing line. The phase separation on the surface and inside the fibers may occur almost simultaneously, thereby leading to the isolated large holes in the core of the fibers.

The organic salt TBAP is generally used to enhance the conductivity of the low polar solvent to increase electrospinnability. In this work, we find that in addition to conductivity enhancement that gives rise to thinner fibers, such as D15T and D30T samples, TBAP can induce a phase separate of the solutions at a lower DMSO fraction. Since TBAP can well dissolve in both CB and DMSO, it is possible that CB and DMSO molecules prefer to interact with TBAP molecules rather than with PS chains in the solutions, which therefore lowers the solvent quality to PS and facilitates the phase separation.

3.4. Superhydrophobicity and Oil Adsorption Capability. We electrospun the PS fibers into nonwoven mats and the water contact angle was measured to investigate the wettability of the mats. Figure 6 shows the representative water drops photograph on spin-cast thin film and the mats formed by nonporous D0T and porous D30T fibers. The water contact angle of PS spin-cast film is averaged 91.9 ± 4.2°, characteristic of a hydrophobic material. D0T nonporous mats shows an averaged contact angle of 136.4 ± 3.2°. The reason for the increase in the contact angle compared to that of spin-cast film is that the stacking of the fibers in the mats creates a great amount of microscale voids between fibers that can trap air to enhance hydrophobicity (Figure 4).[32,33] The averaged contact angles of D20 and D15T mats with nanoscale pore on surface are increased to 148.9 ± 2.1° and 145.6 ± 0.9°, respectively, because the surface roughness makes another contribution to the hydrophobicity. D30, D30T, and D40 mats with microscale pores on fiber surface show even higher averaged contact angles, 155.1 ± 4.8°, 153.8 ± 2.8°, and 152.3 ± 5.1°, respectively, all above 150°, and the water drops can freely roll on the mats, indicating that the roughness created by the combination of the voids between fibers and the microscale pores on the fiber surface can lead to a superhydrophobic surface. The water contact angles of all the fibrous mats are listed in Table 1.

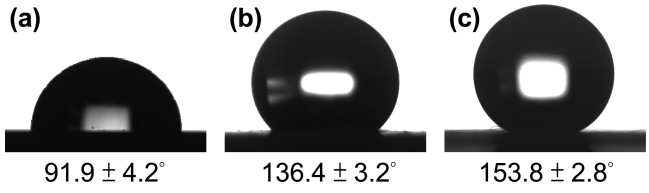

Figure 6. Representative images of the water droplets and the averaged contact angles on the surface of (a) PS spin-cast film, (b) D0T nonporous fibrous mat, and (c) D30T porous fibrous mat.

The oil adsorption capacity was investigated with four common oils, including silicone oil, pump oil, sunflower oil, and diesel. Since PS is a hydrophobic but not an oleophobic material, the PS sorbents can selectively adsorb oil while repel water. The maximum oil adsorption capacities of the fibrous sorbents for the four oils are displayed in Figure 7. D15T and D30T apparently show much higher oil adsorption capacities than others, especially for silicone oil, pump oil, and sunflower oil. The adsorption capacity of the highly porous fibrous sorbents prepared in the present work is up to ~900 g/g for silicone oil, which is much higher than that in the previous studies.[4,5] Taking a detailed look at the data, the adsorption capacity is in the order D30T > D15T > D0T > D20 > D30 for all the four oils. Note that the composition of the D40 solution is too close to the demixing line so that we were unable to steadily collect sufficient fibers for oil adsorption tests. The amount of the oils the sorbents can take is also highly dependent on the type of oils, which is found to follow the order of oil viscosity, i.e., silicone oil (1.021 Pa·s) > pump oil (0.143 Pa·s) > sunflower oil (0.054 Pa·s) > diesel (0.004 Pa·s). The adsorption capacity increases with increasing viscosity is due to a better adhesion of high viscous oils to the fibers.[34]

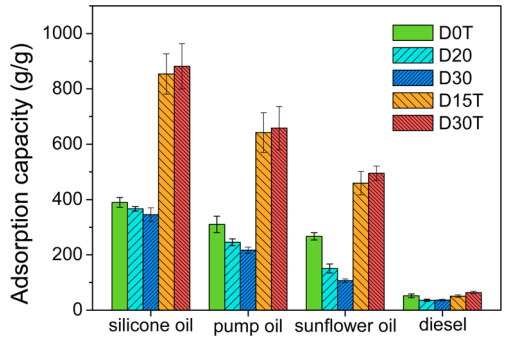

Figure 7. Maximum oil adsorption capacities of the fibrous sorbents for different oils.

For fibrous sorbents, the adsorbed oil is mainly distributed over the fiber surface and trapped in the void space between the fibers, driven by the capillary force to reduce the surface free energy of the fibers. In general, thinner fibers show higher adsorption capacities due to the larger specific surface area. With porous structures, the adsorption capacity can be further enhanced,[5] especially for the holes that grow from the surface

DOI: 10.1021/acs.macromol.6b02696
Macromolecules 2017, 50, 2528−2534

into the core of the fibers. D15T fibers are thin and the nonsolvent-induced holes inside the fibers are slightly open to air, thus providing the conditions for a high oil adsorption capacity. Although D30T fibers are relatively thicker, the holes inside the fibers are large and widely open on the surface, which provide spaces to effectively trap oils and explains why D30T sorbents show the best oil adsorption capacity. The lower adsorption capacities of D20 and D30 are due to the large fiber diameter that reduces the contact area for retaining oils in the voids between fibers despite the existence of the large holes inside the fibers. The fact that D0T mats with smooth fiber surface have a higher adsorption capacity than D20 and D30 apparently results from the small fiber size.

Since the fibrous sorbents fabricated from the solutions with 1 wt % TBAP, including D30T, D15T, and D0T, happen to show higher adsorption capacities, one may wonder whether the interaction between TBAP and oils makes a contribution to the adsorption. To clarify this point, we have used methanol to selectively remove TBAP from the fibrous sorbents, and the adsorption capacities of the sorbents with and without TBAP are found to be identical. The effect of TBAP on adsorption can therefore be ruled out. Also, note that the adsorption capacity of the pore-free fiber D0T is ~400 g/g for silicone oil, higher than the value reported previously in similar fiber conditions.[5] The viscosity of the silicone oil used and the sorbent compactness that depends on the ways to collect fibers and to remove fibrous mats from the substrate may affect the adsorption capacity, which are the possible reasons causing the difference.

The adsorption rate is another important parameter for evaluating the adsorption capability. The dependence of the adsorption capacity with pump oil on contact time for varying fibrous sorbents is shown in Figure 8 in which the slopes of the

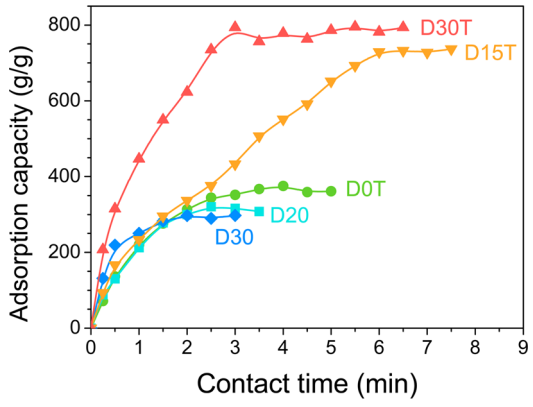

Figure 8. Adsorption capacities as functions of time for the fibrous sorbents with pump oil.

curves reflect the adsorption rates. In the first 30 s, the adsorption rate of D30T is the fastest (600 g/min per gram of sorbent), followed by D30, indicating that the open microscale holes in the fibers are advantageous to rapid adsorption. After 30 s, the adsorption of D30T slightly slows down until saturated at 3 min with a remarkable adsorption capacity. However, D30 sorbent quickly saturates at a low level of adsorption after 30 s, which is again due to the thicker diameter. The smooth fiber, D0T, and the fibers with nanoscale pores on the surface, D20 and D15T, show relatively slow adsorption rates, evidencing that large open holes in the fibers are required to quickly drive the oil into the sorbents regardless of fiber size. It is interesting that although the adsorption rate of D15T is slower, the maximum adsorption capacity reached at 6 min is nearly comparable to that of D30T, indicating that the nanoscale entrance on the surface only slows down the adsorption but does not affect the final equilibrium adsorption capacity. In sum, by simply tuning the fraction of the nonsolvent and organic salt in solutions, fibrous sorbents with extraordinary oil adsorption capacity and controllable adsorption rate can be successfully fabricated through the electrospinning technique.

4. CONCLUSIONS

We have demonstrated that nonsolvents can be incorporated into polymer solutions to successfully electrospin uniform-size hydrophobic fibers with a high fraction of open holes deep into the cores. The nonsolvents should be low volatile so that during the drying process the fraction of nonsolvents increases to cause a phase separation. The effect of the condensed moisture that dissolves in the water-soluble nonsolvent should also involve in the phase separation process. The phase-separated solvent-rich phases give rise to the large holes that grow from surface deep into the fibers after solidification. The macroporous structures greatly increase the roughness of fiber mats, thus leading to a superhydrophobic surface, which provides a superior selectivity of the fibers to adsorb oil while reject water. By optimizing the fiber and hole size to maximize the effective oil-retaining space and oil pathway, the sorbents formed by the fibers show remarkable oil adsorption capacity and rate. The size and the morphology of the fibers can be easily controlled by changing the fraction of good solvents and nonsolvents as well as by adding organic salts that increase the solution conductivity, rendering this electrospinning process a simple method to fabricate highly efficient sorbents for removing oil pollutants over water in spill accidents.

AUTHOR INFORMATION

Corresponding Author

*E-mail: shtung@ntu.edu.tw (S.-H.T.).

ORCID

Shih-Huang Tung: 0000-0002-6787-4955

Notes

The authors declare no competing financial interest.

ACKNOWLEDGMENTS

This work was financially supported by the grant from the Ministry of Science and Technology, Taiwan (MOST 103-2221-E-002-186-MY3).

REFERENCES

(1) Ceylan, D.; Dogu, S.; Karacik, B.; Yakan, S. D.; Okay, O. S.; Okay, O. Evaluation of Butyl Rubber as Sorbent Material for the Removal of Oil and Polycyclic Aromatic Hydrocarbons from Seawater. *Environ. Sci. Technol.* **2009**, *43*, 3846−3852.

(2) Choi, H.-M.; Moreau, J. P. Oil Sorption Behavior of Various Sorbents Studied by Sorption Capacity Measurement and Environmental Scanning Electron Microscopy. *Microsc. Res. Technol.* **1993**, *25*, 447−455.

(3) Li, P.; Qiao, Y.; Zhao, L.; Yao, D.; Sun, H.; Hou, Y.; Li, S.; Li, Q. Electrospun PS/PAN Fibers with Improved Mechanical Property for Removal of Oil from Water. *Mar. Pollut. Bull.* **2015**, *93*, 75−80.

(4) Lin, J.; Shang, Y.; Ding, B.; Yang, J.; Yu, J.; Al-Deyab, S. S. Nanoporous Polystyrene Fibers for Oil Spill Cleanup. *Mar. Pollut. Bull.* **2012**, *64*, 347−352.

DOI: 10.1021/acs.macromol.6b02696
Macromolecules 2017, 50, 2528−2534

(5) Wu, J.; Wang, N.; Wang, L.; Dong, H.; Zhao, Y.; Jiang, L. Electrospun Porous Structure Fibrous Film with High Oil Adsorption Capacity. *ACS Appl. Mater. Interfaces* **2012**, *4*, 3207−3212.
(6) Bognitzki, M.; Frese, T.; Steinhart, M.; Greiner, A.; Wendorff, J. H.; Schaper, A.; Hellwig, M. Preparation of fibers with nanoscaled morphologies: Electrospinning of polymer blends. *Polym. Eng. Sci.* **2001**, *41*, 982−989.
(7) Seo, Y.-A.; Pant, H. R.; Nirmala, R.; Lee, J.-H.; Song, K. G.; Kim, H. Y. Fabrication of highly porous poly (ε-caprolactone) microfibers via electrospinning. *J. Porous Mater.* **2012**, *19*, 217−223.
(8) Nayani, K.; Katepalli, H.; Sharma, C. S.; Sharma, A.; Patil, S.; Venkataraghavan, R. Electrospinning Combined with Nonsolvent-Induced Phase Separation To Fabricate Highly Porous and Hollow Submicrometer Polymer Fibers. *Ind. Eng. Chem. Res.* **2012**, *51*, 1761−1766.
(9) Gupta, A.; Saquing, C. D.; Afshari, M.; Tonelli, A. E.; Khan, S. A.; Kotek, R. Porous Nylon-6 Fibers via a Novel Salt-Induced Electrospinning Method. *Macromolecules* **2009**, *42*, 709−715.
(10) Li, C.-L.; Wang, D.-M.; Deratani, A.; Quémener, D.; Bouyer, D.; Lai, J.-Y. Insight into the Preparation of Poly(vinylidene fluoride) Membranes by Vapor-induced Phase Separation. *J. Membr. Sci.* **2010**, *361*, 154−166.
(11) Srinivasarao, M.; Collings, D.; Philips, A.; Patel, S. Three-Dimensionally Ordered Array of Air Bubbles in a Polymer Film. *Science* **2001**, *292*, 79−83.
(12) Megelski, S.; Stephens, J. S.; Chase, D. B.; Rabolt, J. F. Micro- and Nanostructured Surface Morphology on Electrospun Polymer Fibers. *Macromolecules* **2002**, *35*, 8456−8466.
(13) Lu, P.; Xia, Y. Maneuvering the Internal Porosity and Surface Morphology of Electrospun Polystyrene Yarns by Controlling the Solvent and Relative Humidity. *Langmuir* **2013**, *29*, 7070−7078.
(14) Nezarati, R. M.; Eifert, M. B.; Cosgriff-Hernandez, E. Effects of Humidity and Solution Viscosity on Electrospun Fiber Morphology. *Tissue Eng., Part C* **2013**, *19*, 810−819.
(15) Casper, C. L.; Stephens, J. S.; Tassi, N. G.; Chase, D. B.; Rabolt, J. F. Controlling Surface Morphology of Electrospun Polystyrene Fibers: Effect of Humidity and Molecular Weight in the Electrospinning Process. *Macromolecules* **2004**, *37*, 573−578.
(16) Park, J.-Y.; Lee, I.-H. Relative Humidity Effect on the Preparation of Porous Electrospun Polystyrene Fibers. *J. Nanosci. Nanotechnol.* **2010**, *10*, 3473−3477.
(17) Chang, H.-H.; Beltsios, K.; Chen, Y.-H.; Lin, D.-J.; Cheng, L.-P. Effects of Cooling Temperature and Aging Treatment on the Morphology of Nano- and Micro-Porous Poly(ethylene-co-vinyl alcohol) Membranes by Thermal Induced Phase Separation Method. *J. Appl. Polym. Sci.* **2014**, *131*, 40374.
(18) McCann, J. T.; Marquez, M.; Xia, Y. Highly Porous Fibers by Electrospinning into a Cryogenic Liquid. *J. Am. Chem. Soc.* **2006**, *128*, 1436−1437.
(19) Lin, D.-J.; Chang, H.-H.; Chen, T.-C.; Lee, Y.-C.; Cheng, L.-P. Formation of Porous Poly(vinylidene fluoride) Membranes with Symmetric or Asymmetric Morphology by Immersion Precipitation in the Water/TEP/PVDF System. *Eur. Polym. J.* **2006**, *42*, 1581−1594.
(20) Qi, Z.; Yu, H.; Chen, Y.; Zhu, M. Highly Porous Fibers Prepared by Electrospinning a Ternary System of Nonsolvent/Solvent/Poly(L-lactic acid). *Mater. Lett.* **2009**, *63*, 415−418.
(21) Wei, Z.; Zhang, Q.; Wang, L.; Wang, X.; Long, S.; Yang, J. Porous Electrospun Ultrafine Fibers via a Liquid−liquid Phase Separation Method. *Colloid Polym. Sci.* **2013**, *291*, 1293−1296.
(22) Katsogiannis, K. A. G.; Vladisavljević, G. T.; Georgiadou, S. Porous Electrospun Polycaprolactone (PCL) Fibres by Phase Separation. *Eur. Polym. J.* **2015**, *69*, 284−295.
(23) Washburn, E. W. Note on a Method of Determining the Distribution of Pore Sizes in a Porous Material. *Proc. Natl. Acad. Sci. U. S. A.* **1921**, *7*, 115−116.
(24) Ritter, H. L.; Drake, L. C. Pressure Porosimeter and Determination of Complete Macropore-Size Distributions. Pressure Porosimeter and Determination of Complete Macropore-Size Distributions. *Ind. Eng. Chem., Anal. Ed.* **1945**, *17*, 782−786.
(25) Drake, L. C. Pore-Size Distribution in Porous Materials. *Ind. Eng. Chem.* **1949**, *41*, 780−785.
(26) Choi, J. S.; Lee, S. W.; Jeong, L.; Bae, S.-H.; Min, B. C.; Youk, J. H.; Park, W. H. Effect of Organosoluble Salts on the Nanofibrous Structure of Electrospun Poly(3-hydroxybutyrate-co-3-hydroxyvalerate). *Int. J. Biol. Macromol.* **2004**, *34*, 249−256.
(27) Zong, X.; Kim, K.; Fang, D.; Ran, S.; Hsiao, B. S.; Chu, B. Structure and process relationship of electrospun bioabsorbable nanofiber membranes. *Polymer* **2002**, *43*, 4403−4412.
(28) Klairutsamee, W.; Supaphol, P.; Jangchud, I. Electrospinnability of poly(butylene succinate): Effects of solvents and organic salt on the fiber size and morphology. *J. Appl. Polym. Sci.* **2015**, *132*, 42716.
(29) Fong, H.; Chun, I.; Reneker, D. H. Beaded nanofibers formed during electrospinning. *Polymer* **1999**, *40*, 4585−4592.
(30) Uyar, T.; Besenbacher, F. Electrospinning of Uniform Polystyrene Fibers: The Effect of Solvent Conductivity. *Polymer* **2008**, *49*, 5336−5343.
(31) Reneker, D. H.; Yarin, A. L. Electrospinning jets and polymer nanofibers. *Polymer* **2008**, *49*, 2387−2425.
(32) Ma, M.; Hill, R. M.; Lowery, J. L.; Fridrikh, S. V.; Rutledge, G. C. Electrospun Poly(Styrene-*block*-dimethylsiloxane) Block Copolymer Fibers Exhibiting Superhydrophobicity. *Langmuir* **2005**, *21*, 5549−5554.
(33) Jiang, L.; Zhao, Y.; Zhai, J. A Lotus-Leaf-like Superhydrophobic Surface: A Porous Microsphere/Nanofiber Composite Film Prepared by Electrohydrodynamics. *Angew. Chem., Int. Ed.* **2004**, *43*, 4338−4341.
(34) Johnson, R. F.; Manjreker, T. G.; Halligan, J. E. Removal of Oil from Water Surfaces by Sorption on Unstructured Fibers. *Environ. Sci. Technol.* **1973**, *7*, 439−443.

DOI: 10.1021/acs.macromol.6b02696
Macromolecules 2017, 50, 2528−2534